Stress Topology within Silicon Single-Crystal Cantilever Beam

A.P. Kuzmenko[1], D.I. Timakov[1], P.V. Abakumov[1], M.B. Dobromyslov[2], L.V.Odnodvorets[3]

[1] *South-West State University, 94, 50 Let Octyabtya Str., 305040 Kursk, Russia*
[2] *Pacific National University, 136, Tihkhookeanskaya Str., 680035 Khabarovsk, Russia*
[3] *Sumy State University, 2, Rymsky-Korsakov Str., 40007 Sumy, Ukraine*

Flexural elastic deformations of single-crystal silicon with microspectral Raman scattering are studied. The investigation results are given on nano-scaled sign-changing shifts of the main peak of the microspectral Raman scattering within the single-crystal silicon cantilever beam under influence of flexural stress. The maximum value of Raman shift characteristic of silicon peak equal to 518 cm^{-1}, when elasticity still remains, amounted to 8 cm^{-1}. The qualitative explanation of increase in strength of the cantilever beam due to its small thickness (2 μm) is provided, which is in accord with predictions of real-world physical parameters that were obtained in software environment SolidWorks with the module SimulationXpress.

Keywords: Raman scattering spectroscopy, Silicon single-crystal, Flexural stresses, Mapping of Raman shift distributions.

PACS numbers: 46.70.De, 68.55.jk, 81.05. – t

1. INTRODUCTION

Extension of the well-known in microelectronics Moor's law to nano-scaled domain, when the density of structural components of microchips reached 1×10^8 transistors per square inch, has made the application of nondestructive testing pertinent [1-6]. Special urgency is acquired by the tools on the basis of electromagnetic radiation in both X-ray range (small angle X-ray scattering technique [1] and further up to the infrared (IR) (Raman and IR spectroscopy [2, 3]). Raman spectroscopy (RS) of semiconductor materials makes it possible to obtain data on phonon frequencies, energies of electron states and electron-phonon interactions, carrier concentrations, content of impurities, crystal structure, crystal orientation, temperature, mechanical stresses. RS is increasingly becoming pertinent, which is dictated by considerable complications of technological solutions (beam- and ion-implantation doping, for example) in creating an electronic component base of new generations, especially in nanoelectronics, nano- and microelectromechanical devices, the so called NEMSs and MEMs. With decreasing operating size of components the appearance of elastic stresses is observed, which greatly influences service and functionality characteristics of newly-designed micro- and nano-components.

MicroRaman spectroscopy (MRS) makes it possible to investigate mechanical stresses in many-layered components of microchips. For instance, in microchip with Si_3N_4 strips the size of 240×50 nm, which were separated from the silicon substrate by nanolayers of SiO2 and polycrystalline silicon (10 nm thickness and 9.4 μm width), the Raman shift found amounted to $\pm 4 \text{ cm}^{-1}$ [2], which attested to the practical utility of nondestructive testing. In significantly integrated phototransducers on the basis of single- or polysilicon doped with B or Al atoms, with the help of MRS and micro photoluminescence (resolution of up to 500 nm) the interaction of optical phonons with defects stemmed from compression or tensions, which are not detected by other techniques [3], has been studied. It is well known that the efficacy of photo elements on Si increases with the electrochemical polishing. MRS at nanocrystal pores formed in this case is characterized by the fact that the shape of the peaks tend to be of the Lorentz form and the peak for Si at 520.5 cm^{-1} is slightly shifted. These changes are attributed by the quantum size of the pores [5].

The effect on the Raman shift by one-axis compression stresses in single-crystal silicon was studied in [6]. Stresses in a film the size of 3 inches and 600 nm in thickness were produced by pressing it to the cylinder surface of a large radius (from 0.5 to 1 m). For the cylinder of 05. m radius the shift reached 0.4 cm^{-1} at laser excitation at $\lambda = 325$ nm with a penetration depth into silicon of 9 nm. Distributions of Raman shift feature clarity and are informative in contrast to IR and electron microscopy, X-ray analysis used to this end. In [6] the silicon plate surface (111) nanostructured with ultra short pulses of an excimer laser was studied with MRS. Appeared stresses are given as microdistributions of RS, indicating localization of hexagonal Si (510 cm^{-1}) и α-Si (490 cm^{-1}).

As shown in [7], the effect of ultrasound waves on silicon single crystals with whole conductivity dictates decrease or increase in density of surface charge states. In addition, there is a rearrangement of energy spectrum in surface states. Those changes are explained by modification of defect subsystem in surface layers of crystal silicon, which is associated with redistribution of impurity atoms and production of new defect entities.

Reversibility of the elastic properties of single crystal ZnS at one-axis deformation [8] was explained by data of electron paramagnetic resonance. It was established that when ZNS samples with paramagnetic impurity Mn^{2+} ions in all site types were deformed, the lines became wider and shifted. The observed changes are associated with variations of distances between the lattice sites. Sample deformations (up to pressure of 102 MPa) were done immediately within a radiospec-

trometer resonator, which produced data that corroborated the appearance of shifts and change in peak shapes between Lorentz and Gauss forms, which disappeared with magnetic fields turned off.

The effect of elastic deformations on phonon spectrum characteristic of NaCl was studied in [9] by computer simulation. The model predictions were carried out by the molecular dynamics method. In this case, two modes of crystal deformations were considered, namely, all-round tension-compression and pure shear. It is shown that they cause the transformation of phonon state density. However, localized vibration modes, the so called discreet brizers, depend only on the first type deformation, whereas the shear deformation does not influence them. It is noted that in determination of mechanical features of single crystals by indentation method under load within the range $0.1 \leq P \leq 1$ N at the formation of the indenter footprint just elastic deformation manifests itself. This is shown in [10] with an example of alkali-halide single crystals, such as LiF, KCl and NaCl the size of $4 \times 8 \times 20$ mm. In this case the amount of elastic deformation is significantly decreases when the Young modulus of the crystal studied increases.

Nondestructive nature of MRS made it possible to visualize so much unique microobject as domain wall in magnetically-ordered materials, including $YFeO_3$ [11]. The hyperspectral distributions of intensity variations of MRS at 221 cm^{-1} line for Fe^{3+} made it possible to detect both features of fine structure of the domain wall and the rotation of magnetization within it, that is to examine its fine structure. That has allowed one in the central part of the domain wall, for the first time, to record an area with zero magnetization.

The work presents the results of nano-scaled studies of sign-changing shifts of the typical for Si peak of Raman scattering 518 cm^{-1} that originate within the cantilever beam at flexural deformations. The maximum change of sign of appearing deformations is concentrated in the cross-section of the beam (with the minimum size of 2 µm). The model predictions of deformations were done and comparative analysis of mechanical property changes of the deformed single-crystal silicon in response to flexural stresses is carried out.

2. EXPERIMENTAL SECTION

The present paper deals with such model material as single crystalline silicon, which has in the RS spectrum one clear line, namely, 518 cm^{-1}. Studied was a console beam of the cantilever with microscopic sizes of $135 \times 35 \times 2$ µm, typical of cantilevers.

To examine distributions of micro- and nanostresses in the beam a confocal microscope and Raman microspectrometer OmegaScope together with atomic force microscope (AFM) (AIST-NT, Zelenograd-city, Russia) were used. The confocal microscope made it possible to choose the area for precise positioning of the exciting radiation of a semiconductor laser on the deformed beam. The study with MRS was done at $\lambda = 473$nm with a power of 25 mW and a spatial resolution of 425 nm. The microspectrometer provided spectral resolution as low as 0.8 cm^{-1}. Flexural deformations were recorded

with the confocal microscope. The area of measurements on the cantilever beam was chosen with the confocal microscope ($\times$ 10 lens) with a numerical aperture of 0.28. The optical resolution made it possible, in a precision way, to visualize and choose an area for construction of maps of hyperspectral distributions for Raman shift with various levels of beam bending.

For studying flexural deformations of silicon two semicontact fpN11 cantilevers with a rigidity of 5.3 N/m were used. The first (tested) was fixed in the holder of AFM. Another one acted as a stop. For this purpose, it was rigidly fixed on a scanator (Fig. 1a) and was able to micrometrical move in a desired direction, causing beam flexural deformations of the cantilever at rest. The scanator motion was set programmatically. The motion step was set with consideration for minimum measurement level of RS lines and hardware spectral resolution (0.8 cm^{-1}) and was equal to 20 µm. The real-world bend of the beam is given by its confocal image (Fig. 1b).

Maximum motion of the free end of the beam was more than 100 microns. All the time the beam deformation continued to be elastic, which was confirmed by its return to the original position after the load has been removed. The maximum beam bending was at 4.5 GPa.

Mapping of MRS spectra was done with the stepper motor of the atomic force microscope. Hyperspectral data at the silicon characteristic line of 518 cm^{-1} were obtained with 100x lens having a numerical aperture of 0.7. It should be noted that the scanning region of the cantilever in the AFM (100×100 µm) considerably surpasses the cross-section of the beam. This allowed one , with the system of piezo drives motion of the positioner and input-output of radiation with a step of 0.6 µm


a)

b)
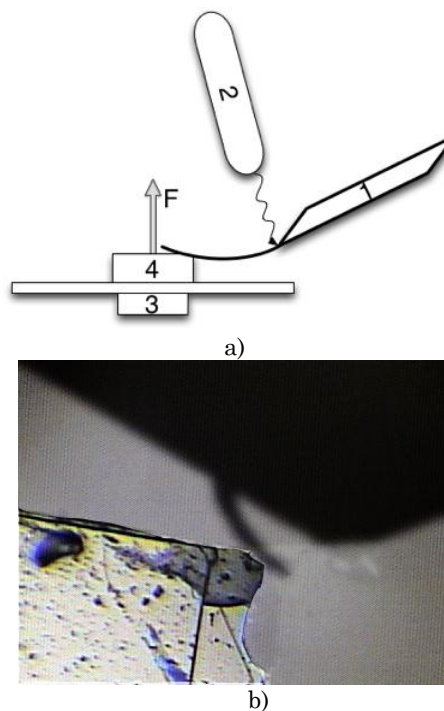
Fig. 1 – A schematic image of flexural deformation of the cantilever beam (a) and its optic image in the confocal microscope (b). 1 – the cantilever beam (the first); 2 – source and exciting laser radiation; 3 – a scanator with a table for the sample; 4 – stop from cantilever (the second)

within the field of 30×30, to construct the array from 900 spectra in MRS (Figs. 2, 3a, 4). With these data, the map of elastic stress distribution within bended part of the beam along its sides with the size of 35 and 2 μm was constructed.

At first stage the MRS distribution was studied along the longest side of the beam (135 μm), which made it possible to establish the area of its maximum deformation. It is found that the area does not exceed its third part in size (Fig. 2). Further the detailed examination of hyperspectral distributions was made just in this area.
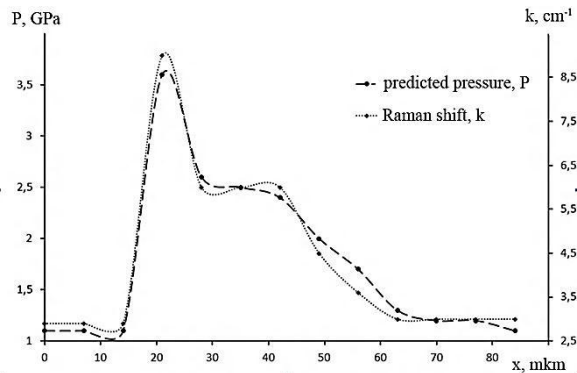
Fig. 2 – Distribution of Raman shifts and pressures across the axis along the longitudinal plane of the beam


a)

b)
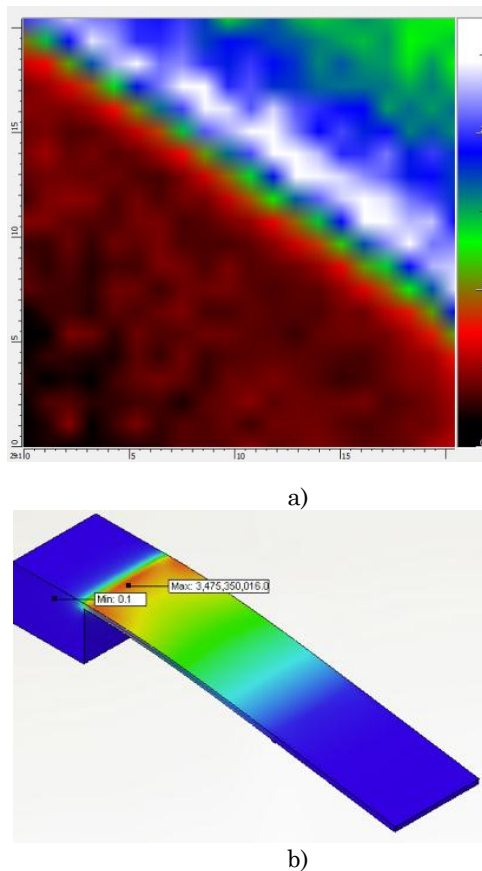
Fig. 3 – Distribution of stresses across the cantilever beam according to MRS (a) and model predictions (b)

The maps of stress distributions by hyperspectral data of MRS within the cantilever beam were con-

structed both along the maximum plane the size of 35 μm (Fig. 3a) and in the cross-section the size of 2 μm (Fig. 4a and b). Fig. 3b presents the image of predicted distribution of flexural deformations along the beam in the area immediately adjacent to the base of the cantilever chip in the scale of 32×12 μm. The magnitude of elastic stresses reached maximum value immediately in the fastening area of the beam cantilever.

Model distributions of elastic stresses and load are carried out according to fon Mizes approach without consideration of sign of their changes. Considered are the resulting stresses when the entities with set geometrical parameters and pertinent characteristics are influenced by the arbitrarily directed elastic actions. The actions along each of six degrees of freedom characterizing any solid body in one-axis approximation are substituted with an equivalent stress.

Calculations were done within software environment SolidWorks for the real-world physical parameters, size, and taking into consideration how the fastening area of the cantilever beam influences the beam bending. The produced stresses were analyzed with the module Simulation Xpress. As a result, established were both critical areas of stresses and levels of strength. As is seen from the model predictions given in Fig. 3a and b, and Fig. 4 the distributions of elastic stresses within the cantilever beam are in good comparison with the experimental results obtained by the hyperspectral data of MRS.

a)

b)
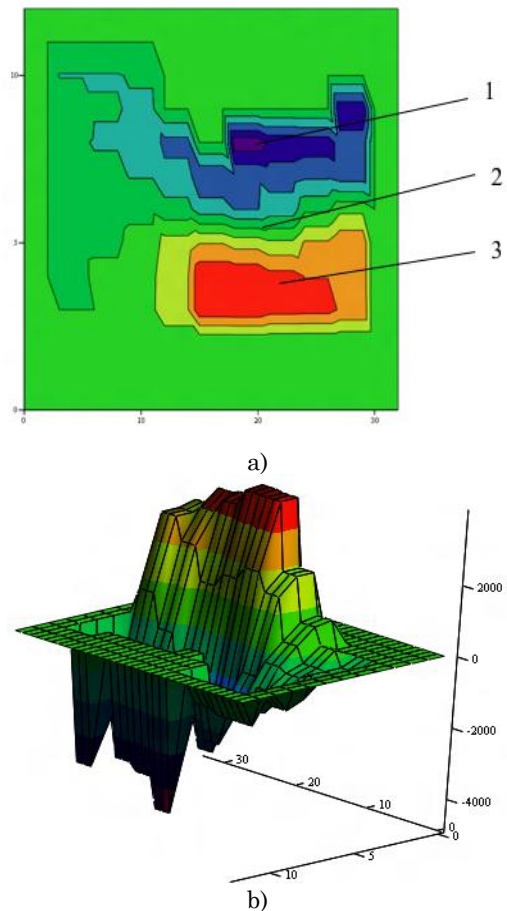
Fig. 4 – The distribution of flexural stresses in the transverse plane of the cantilever beam according to the MRS: a – three-dimensional, b – a planar (compression – 1, stretching – 2 and undeformed region – 3)

As the MRS data indicate, in the distribution of flexural stresses across the cantilever beam the sign of deformations changes (Fig. 4a), which is most vividly demonstrated by their three-dimensional image of distributions according to MRS. The analysis of set of calculated values and directions of elastic stress vectors obtained for the base of the cantilever beam clearly demonstrates nature of their variations. Even slight elastic stresses in the base of the beam in chip are of alternating character. In the beam itself, the elastic stresses are of clear-cut antiphase character. It is characteristic that along the middle line in the cantilever beam the amount of stresses decreases considerably down to zero.

3. RESULTS AND DISCUSSION

To explain data on flexural micro stresses within the cantilever beam one must take into consideration that in the most general analysis the signal intensity of MRS is dictated by the amplitude of coming(E_i) and scattered (E_s) light wave and also by the Raman tensor (R_j):

$$I = C\Sigma |e_i R_j e_s|^2, \qquad (1)$$

where C is the dimensional factor. For the silicon single crystal studied with the typical for semiconductors orientation (100) with consideration for geometry of applied flexural stresses the Raman tensor, that has 9 components, is dramatically simplified, which provides, as a result, only one line in the MRS spectrum, namely $518\,cm^{-1}$. In our case all examinations were conducted with respect to the base line, which makes it possible to apply inferences of [3]:

$$\Delta\omega = [pS_{12} + q(S_{11} + S_{12})]\sigma / 2\omega_0. \qquad (2)$$

Taking into account the well-known for silicon magnitudes of elastic constants $S_{11} = 7.68 \times 10^{-2}Pa^{-1}$, $S_{12} = -2.14 \times 10^{-12}Pa^{-1}$, $p = 1.43\omega_0^2$ and $q = -1.889\omega_0^2$ for the maximum value of the Raman shift obtained, which was equal to $9\,cm^{-1}$, by using (2) one is able to calculate the corresponding value of applied flexural stress, namely $\sigma = \Delta\omega / 2 \times 10^9 Pa = 4\,GPa$. Therefore, the experimental data on elastic stresses within the cantilever beam are in good agreement with theoretical inferences.

Cantilever beam with a typical transverse size (2 μm) can be thought of as the object that occupies an intermediate position between the single crystal and microcrystalline structures. For objects of this type there are significant changes in mechanical properties due to size effects [9-12]. In analyzing the observed increased strength of the cantilever beam with respect to flexural deformations, we will take into account both its strengthening due to dislocation-kinetic mechanism and changes in lattice parameters. In both cases, with increasing strength of mono-and nanocrystalline materials dictated by the size effect embrittlement is observed [12, 13].

The existence of sign-changing flexural stresses in the cantilever beam (Fig. 4a), when concurrently, in the area of $d = 2$ μm, there are both compression stress and tensile stress, in itself provides a unique combination,

which is of great importance for the analysis. The area of critical bend of the cantilever beam (*L*) is localized (Fig. 1b) at a distance on the order of several tens of micrometers from its body. In this case the value of ratio $R = L / D$ may be decreased by almost an order of magnitude. According to [9], in micro- and nanocrystals this brings about the size effect of strength increase ($\sigma \sim D^{-0.6 \div 1.0}$), which interferes with plastic deformations. At the boundary with small *R*, the mechanism of deformation strengthening operates due to dissipation of elastic energy at the dislocations accumulated in this area, which follows from the dislocation-kinetic approach. The value of maximum shift in the MRS spectrum, when the beam still maintains elastic properties (Fig. 2), was 2 %, which can be thought of as the bending yield point for the given *R*, at which, according to [10],]: $\sigma = D^{-0.75}$. From this it follows the practical recommendations to cantilever manufactures, namely, in order to increase the magnitude of σ one must decrease the beam width from the current 35 μm by an order of magnitude, which will provide both increased sensitivity of atomic-force microscopy and the prolonged service life of cantilevers themselves.
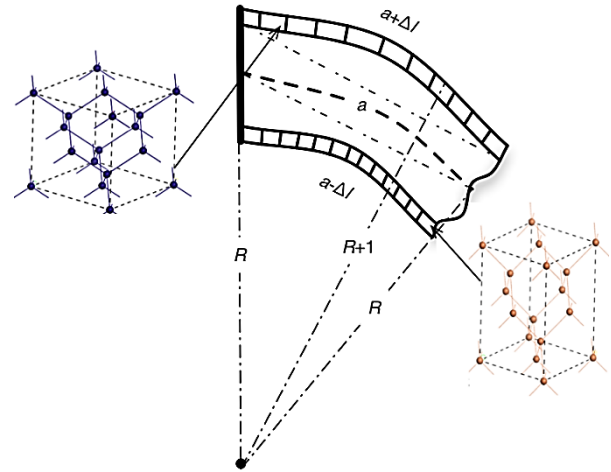
Fig. 5 – Size changes in the transverse plane of the cantilever beam and schematic images of silicon lattice cells at a flexural stress of 4.5 GPa in the area of compression and tension

To further analyze data obtained on the distribution of MRS consider the part of the beam that was undergone, to the greatest extent, to the flexural deformations. As is seen from Fig. 4, along the beam axis there is no deformation under the influence of flexural stress. At the same time, its top surface is stretched, but down surface is compressed by the magnitude of Δ*l*. If one considers the width of the deformed region along the beam being a, then the elongation per unit length Δ*l* can be determined from Fig. 5. Taking into consideration similarity of triangles formed by radii *R* and *R* + 1 and arc chords *a* и *a* + Δ*l*, let us write down their ratios $R / (R + 1) = a / (a + \Delta l)$. Taking all of this into account, the amount of deformation derived with substitution of real-world size of the cantilever beam is equal to 2.2 %. It should be remembered that the flexural deformation of the beam under study is elastic. Clearly, under such conditions, the maximum value of the line shift (for the peak pertinent to $518\,cm^{-1}$) in the MRS spectrum makes it possible to evaluate the

magnitude of ultimate strength σ and the magnitude of deformation, which also turned out to be of the order of 2 %.

Since the binding energy of Si-Si in the single crystal of silicon is comparatively low (176 kJ / mol), in the elasticity area compression and tension should be accompanied by the corresponding changes of the crystal lattice parameters [8]. The analysis of deformational changes of silicon crystal lattice with the characteristic period of 5.4307 Å carried out with mathematical package Material Studio and the Broiden-Fletcher-Goldfarb-Shanno algorithm provided for experimentally determined flexural stress of 4.5 GPa the value of lattice period of 5.3195 Å. Hence, the period was de-creased by 2 %, which, in essence, coincided with the elongation per unit length Δl (Fig. 5) and with found shift of the line in hand in the MRS spectrum.

4. CONCLUSIONS

In sum, the use of methods of microspectral Raman analysis for studying micro- and nanoobjects both opens up additional opportunities for investigation at considerable deformation actions and makes it possible to devise novel methods of nondestructive testing of mechanical properties for solids. The data acquired in this case may be used with success for modeling deformation processes in various solid materials.

REFERENCES

1. D.L. Williamson, *Sol. Energ. Mater. Sol. C.* **78**, 41 (2003).
2. Ingrid De Wolf, *Semicond. Sci. Technol.* **11**, 139 (1996).
3. P. Gundel, M.C. Schubert, F.D Heinz, R. Woehl, J. Benick, J.A. Giesecke, D. Suwito, W. Warta, *Nanoscale Res. Lett.* **6**, 197 (2011).
4. C. Himcinschi, M. Reiche, R. Scholz, S.H. Christiansen, U. Gosele, *Appl. Phys. Lett.* **90**, 231909 (2007).
5. R.S. Dubey, D.K. Gautam, *J. Optoelectron. Biomedical Mater.* **1**, 8 (2009).
6. M.S. Amer, L. Dosser, S. LeClair, J.F. Maguire, *Appl. Surface Sci.* **187**, 291 (2002).
7. N.N. Zaveryukhina, E.B. Zaveryukhina, S.I. Vlasov, B.N. Zaveryukhin, *Tech. Phys. Lett.* **34**, 241 (2008).
8. S. Omel'chenko, M. Bulanyi, *Phys. Solid State* **39**, 1091 (1997).
9. S.V. Dmitriev, Yu.A. Baimova, *Tech. Phys. Lett.* **37**, 451 (2011).
10. V.A. Feodorov, L.G. Kariev, A. Glushkov, *Tech. Phys.* **47** 866 (2002).
11. A.P. Kuzmenko, P.V. Abakumov, M.B. Dobromyslov, *J. Magn. Magn. Mater.* **324**, 1262 (2012).
12. G.A. Malygin, *Phys. Solid State* **54**, 1606 (2012).
13. O. Chaojun, Li Zhenhuan, H. Minsheng, H. Lili, H. Chuantao, *Mater. Sci. Eng. A* **526**, 235 (2009).